Initial Results from the Helios-1 Search-Coil Magnetometer Experiment

F.M. Neubauer[1], H.J. Beinroth[1], H. Barnstorf[1], and G. Dehmel[2]

[1] Institut für Geophysik und Meteorologie, TU Braunschweig,
Mendelssohnstr. 1A, D-3300 Braunschweig, Federal Republic of Germany
[2] Institut für Nachrichtentechnik, TU Braunschweig,
Mühlenpfordtstr. 23, D-3300 Braunschweig, Federal Republic of Germany

Abstract. The Helios search-coil magnetometer experiments provide a unique potential for studies of electromagnetic plasma wave modes in the solar wind between 0.3–1 A.U. because of excellent background noise levels, high time-resolution and high accuracy. Daily average spectral densities ($\gamma/\sqrt{Hz}$) in the frequency range from 4.7 Hz–220 Hz show a pronounced increase as the sun is approached with complex superposed variations. Their values have a range of more than an order of magnitude. The shock of January 6, 1975 provides an interesting example for the use of high time-resolution spectral data. The fine structure and the long term variations in wave fields after the perpendicular shock are discussed. Also two interesting examples of "magnetic holes" are presented.

Key words: Magnetic fluctuations in the solar wind — Helios search-coil magnetometer.

1. Introduction

The Helios search-coil magnetometer experiment has been designed to observe the high-frequency component of magnetic fluctuations in the interplanetary medium in the frequency-range from about 4 Hz–2.2 kHz. This frequency-range has been chosen such as to allow observations up to the maximum expected electron gyro frequency on the orbit of Helios. To fix ideas note that at 50γ the electron gyro frequency $f_{ce} = 1.4$ kHz. From a plasma physics point of view the observed fluctuations may be due to Doppler shifted Whistler waves or convected non-propagating structures. A more detailed discussion of this point is contained in Neubauer et al. (1977).

The experiment has the following scientific objectives:

1. Observation of the background interplanetary magnetic fluctuation levels in relation to macroscopic features like high-speed streams, shock-flow systems (as opposed to shock fine structure).

2. Study of the plasma physics of shocks, rotational and tangential discontinuities and other short time-scale phenomena.

3. Search for wave phenomena at high frequencies not connected with local plasma-and-magnetic field features particularly close to the sun.

Interesting examples of the wave phenomena connected with directional discontinuities, shocks and small "magnetic holes" (e.g. Turner et al., 1976) have been reported in a more specialized publication (Neubauer et al., 1977).

In this paper we shall present an overview of the average fluctuation levels observed during a time period from mid-January 1975 through March 1975 as a first contribution to objective one. In addition we shall discuss the magnetic wave phenomena observed in connection with the shock of January 6, 1975 and its flow system.

2. Instrumentation

Helios-1 has been launched on December 10, 1974 into an orbit with a perihelion of 0.31 AU. Helios-2 has been launched on January 15, 1976 with a perihelion of 0.29 AU. The pay-load of the two spacecraft includes almost identical search-coil magnetometer experiments which are still operating and providing excellent data at the time of this writing.

A detailed technical description of the search-coil magnetometer experiment has been given in the paper by Dehmel et al. (1976). We shall here summarize a few essential features with the aid of Figure 1. Each instrument consists of three orthogonal search-coil sensors with the Z-axis parallel to the spin-axis and the X- and Y-axis in the equatorial plane. The output voltage of each sensor-preamplifier unit is proportional to the time derivative of the component under consideration i.e. $\dot{B}_x$, $\dot{B}_y$, $\dot{B}_z$. The essential part of the on-board data processing system is the spectrum analyzer. It consists of two sets of eight bandpass filters spaced logarithmically in frequency with the center frequencies f_{cn} given in the figure. One of the filter sets is used for the Z-sensor output, the other one for the X or Y-component. The filter outputs are squared and averaged by a digital mean-value-computer over successive time intervals of length T_A. For most of the primary mission of Helios-1 $T_A = 1.125$ s. For the same time interval T_A the peak reading from each filter output is also obtained and transmitted to the earth in addition to the mean square values M_n. All the filters are processed in parallel. Use of the digital mean-value-computer guarantees an accuracy for the power spectral density estimates not achieved by interplanetary wave experiments in the past. The mean square values M_n are related to the power spectral density $P(f)$ of a given component of the magnetic field by

$$M_n = \int_0^\infty |T_n(f)|^2 f^2 P(f) \, df, \tag{1}$$

where $T_n(f)$ is the complex transfer function of filter n which quickly tends to 0 beyond the 3dB-points for each filter as shown in the inset of Figure 1. The power spectral densities $\bar{P}_n$ or square-roots thereof assigned to the center

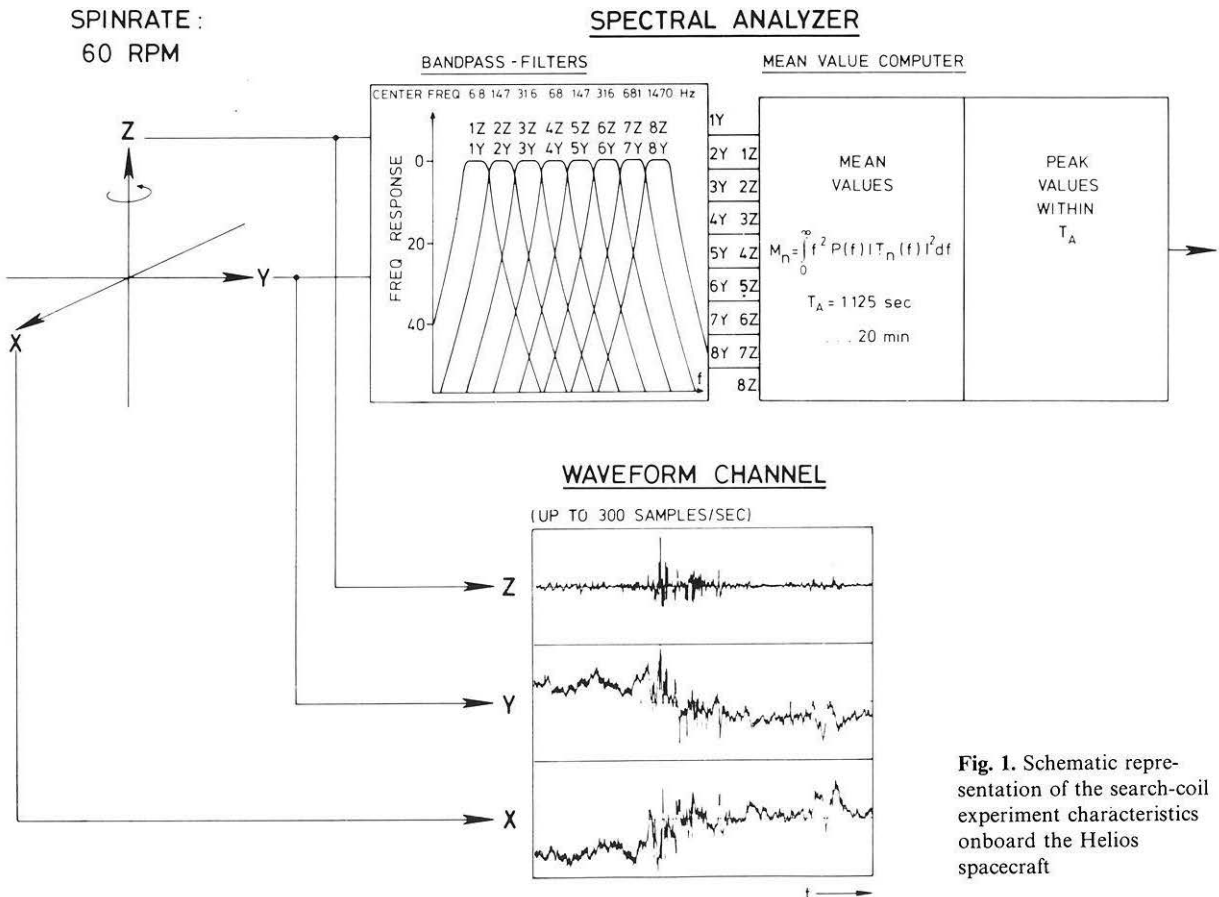# SEARCH-COIL ON-BOARD DATA PROCESSING

SPINRATE : 60 RPM

SPECTRAL ANALYZER

BANDPASS - FILTERS

CENTER FREQ 68 147 316 68 147 316 681 1470 Hz

1Z 2Z 3Z 4Z 5Z 6Z 7Z 8Z
1Y 2Y 3Y 4Y 5Y 6Y 7Y 8Y

FREQ RESPONSE

0

20

40

MEAN VALUE COMPUTER

MEAN VALUES

$$M_n = \int_0^\infty f^2 P(f) |T_n(f)|^2 df$$

$T_A = 1125$ sec

.... 20 min

PEAK VALUES WITHIN T_A

WAVEFORM CHANNEL

(UP TO 300 SAMPLES/SEC)

Z

Y

X

Fig. 1. Schematic representation of the search-coil experiment characteristics onboard the Helios spacecraft

frequencies f_{cn} in this paper are given by

$$\bar{P}_n = \frac{M_n}{\Delta f_n f_{cn}^2} = \int_0^\infty |T_n(f)|^2 (f/f_{cn})^2 P(f) \frac{df}{\Delta f_n}$$

or

$$\bar{P}_n(f_{cn}) \approx \int_{f_{ln}}^{f_{un}} P(f) (f/f_{cn})^2 \frac{df}{\Delta f_n}$$

(2)

because of the high quality of the filters. Here $f_{\mathrm{l}n}$ and f_{un} are the lower and upper frequency limits (3 dB-points) of filter n, respectively, and $\Delta f_n = f_{un} - f_{\mathrm{l}n}$ is the bandwidth. The square-root of $\overline{P}_n(f_{cn})$ will be displayed in all plots in this paper.

In our studies of short time-scale phenomena later in this paper we shall sometimes need the mean squared time derivative of a magnetic field component e.g. B_z in a given frequency band. Using Equations (1) and (2) we obtain

$$\frac{1}{T_A} \int_0^{T_A} (\dot{B}_z)^2 \, dt = \dot{B}_z^2(N, M) = 30.77 \times \left\{ \sum_{n=N}^{M} f_{cn}^3 \, \overline{P}_n(f_{cn}) \right\} \tag{3}$$

where $\overline{\dot{B}_z^2}(N, M)$ is the contribution to the overall $\overline{\dot{B}_z^2}$ by filters N through M.

In case of the availability of high data transmission rates wave form data can be transmitted to the ground at rates of up to 57 vectors/s. More precisely, in the waveform channels the outputs from the three orthogonal sensors are transmitted after appropriate filtering etc. In the case of Helios-1 the waveform vector data represent the magnetic field vector **B** in the frequency band from 4 Hz to approximately half the sampling frequency. In the case of Helios-2 the waveform vector data represent the time derivative $\dot{\mathbf{B}}$ of the magnetic field vector in the same frequency ranges as on Helios-1 i.e. analog integration circuits used on Helios-1 have been omitted on Helios-2.

In a special memory mode initiated by an on-board event detector wave form data at rates up to 300 vectors/s can be obtained for short time intervals.

An outstanding feature of this experiment is the low background noise level (see Neubauer et al., 1977) which allows the continuous observation of interplanetary magnetic fluctuations in the lower frequency channels 1 Z–5 Z and 1 Y–5 Y even at 1 AU. This is due to the magnetic cleanliness of the spacecraft and the low sensor-preamp noise levels.

Daily Averages of Spectral Densities

To obtain an overview of the spectral densities observed we have computed daily averages of the spectral densities in the frequency channels centered at 7 Hz, 15 Hz, 32 Hz, 68 Hz and 147 Hz for the Z-component and the Y-component which give essentially identical results. By spectral density (measured in $\gamma/\sqrt{\mathrm{Hz}}$) we always mean the square-root of the power spectral density $P(f)$ which is measured in γ^2/Hz. Averages are always square-roots of averaged power spectral densities or equivalently Pythagorean spectral density averages.

The results for the time interval from January 19, 1975 to April 5, 1975 are plotted in Figure 2 on a logarithmic scale for several solar rotations. Relative heliographic longitude is based on the Carrington rotation period. The origin has been chosen to make best use of the space in the figure. The radial distance variation is also indicated in the figure. On the right hand side the background noise levels of the various channels are indicated. The background noise values have not been subtracted from the averaged power spectral densities. Except for a few days it is only channel five which is affected by the background noise levels in the upper panel of Figure 2.
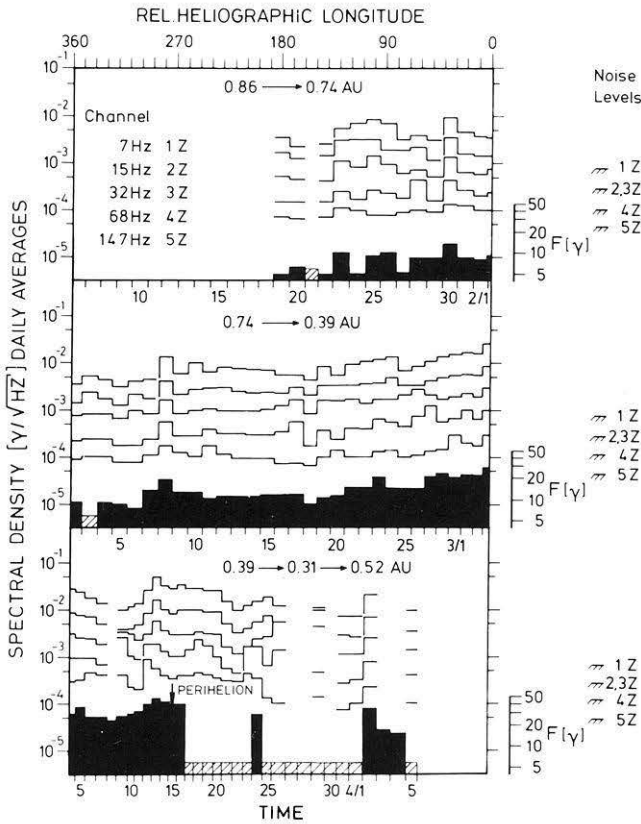
Fig. 2. Daily average spectral densities for channels $1Z$, $2Z$, $3Z$, $4Z$ and $5Z$ as a function of time or relative heliographic longitude from January 19 to April 6, 1975. Magnitudes of daily magnetic field averages are also shown for most days. Days with insufficient data for the computation of averages are shown cross-hatched

We have used heliographic longitude as an independent variable and we have plotted daily average magnitudes of the magnetic field to aid in finding relationships between the corotating macrostructure of the magnetic field measured by the flux-gate and the high-frequency wave fields observed by the search-coil wave experiment. Inspection of the magnetic field averages since launch clearly reveals corotating structures the properties of which vary as a function of distance from the sun. In this comparison it has to be taken into account that the corotating features in $|\mathbf{B}|$ are aligned along spirals details of which will be presented in a future publication. A simultaneous variation in heliographic latitude makes the situation even more complicated. The wave fields do not show a clear behavior of this type although a few corotating features may be present. However, it is interesting to note that the outstanding maxima in spectral density on January 30, February 8, March 4, March 13 and April 2 are always connected with maxima in magnetic field magnitude. The reverse is not true.

As expected there is a clear increase in spectral densities as the sun is approached. For example, in channel $1Z$ the spectral density varies between 2×10^{-3} to 8×10^{-3} $\gamma/\sqrt{\text{Hz}}$ in the upper panel of Figure 2 corresponding to 0.86–0.74 AU. Near the sun from 0.39 AU–0.31 AU the spectral density varies between 10^{-2} and 5×10^{-2} $\gamma/\sqrt{\text{Hz}}$.

Concerning the frequency dependence of the spectral densities we note that positive slopes do not occur in the daily average spectra. Sometimes regions with small negative slope or zero slope are found as on days February 26 between about 15 and 32 Hz, March 9 between about 15 and 68 Hz and March 23 between about 32 and 68 Hz. Apart from this clustering of spectra with small negative slope close to the sun the spectral characteristics of the daily averages only change in a minor way as a function of distance. If we relate the spectral densities for channels $1Z$ and $4Z$ by a power law $\sqrt{\overline{P(f)}} \sim f^{-\alpha}$ the spectral index α varies from 0.9–1.6 in the upper panel of Figure 2 corresponding to 0.86–0.74 AU. In the lower panel it varies from 0.6–1.5 between 0.39 and 0.31 AU.

We have noted in the previous paper on Helios results (Neubauer et al., 1976) that in one-hour-plots a slowly varying component with a time scale of several minutes and longer can generally be distinguished from so-called events" with time scales of a minute and loss due to discontinuities, "magnetic holes" etc. The overall daily averages considered here are sometimes determined by large events and sometimes by the slowly varying component only. For example, the maximum on March 13 is essentially determined by half a day of large slowly varying component. March 11, 1975 with only a minor daily average contains the most dramatic "events" of the primary mission of Helios-1 except for the shocks of January 6 and 8, 1975.

We conclude this section with a brief discussion of the physical explanation of these results. For the source location there are 2 general possibilities: The source may be a local one or at some distance from the location of observation. Since visual inspection of 24h-plots and 1h-plots reveals no evidence for frequency dispersion we favor the former alternative i.e. a local origin of these fluctuations. There are several interesting candidates for a local wave source. First, thermal magnetic fluctuations which would be extremely small for an equilibrium plasma are enhanced appreciably for distribution functions near marginal instability or even in the instability regime. Such distribution functions are encountered in the solar wind (see e.g. Hollweg, 1975). Also these fluctuations may be produced by nonlinear cascading of high amplitude and long period waves. Third, the possibility cannot be excluded that we are dealing with convected electron structures (Lemaire and Burlaga, 1976). Firm conclusions on the applicability of these ideas can only be reached after further detailed observational analysis including plasma data.

The Shock of January 6, 1975

The fine structure of collisionless shocks is still one of the most interesting problems of plasma physics. For a recent review see Galeev (1976). Briefly the physical problem can be described as follows. An ideal nonlinear compression

wave in a magnetoplasma is known to steepen as time progresses. In collision dominated magnetogasdynamics the steepness is finally limited by internal friction and other dissipative processes. Since the steepening can be visualized as the generation of short wavelength wave energy in the overall spatial spectrum describing the nonlinear wave we can say that finally these newly generated short wavelength components are dissipated at the same rate as they are generated. The dissipation is determined by collisions in this case.

In the collisionless case where the collision frequencies are negligible compared with all other characteristic frequencies of the magnetoplasma the steepening may finally be limited by the propagation of short wavelength waves away from the steepening region due to dispersion effects. Depending on the precise initial conditions this basic mechanism may be modified or even replaced by the onset of microinstabilities during the steepening. Also macroinstabilities may play an important role as for example the nonlinear decay instability. Obviously waves play an important role in the physics of collisionless shocks. Therefore they are an important diagnostic tool for the study of collisionless shocks. Apart from the waves in the "wake" region downstream of the shock waves may propagate in the upstream direction or they may be excited by fast particles moving in the upstream direction. The latter waves are generally referred to as "precursors".

A large number of possibilities exists for the shock structure which finally arises. It depends on a number of important dimensionless parameters: β the ratio of total plasma pressure over magnetic field pressure, the angle θ between the shock normal and the magnetic field vector ahead of the shock, the Alfvén Mach number M_A (say), the ratio of electron and ion temperature T_e/T_i, the mass ratio m_e/m_i, collision frequency divided by plasma frequency $v_{ei}/\omega_{pe} \ll 1$, plasma frequency over electron gyro frequency (say) etc.

A considerable fraction of the parameter space β, θ, M_A, T_e/T_p etc. can be investigated experimentally in the laboratory. Laboratory studies and shock investigations in space plasmas like the plasma of the solar wind can complement each other in an important way (Schindler, 1969). Generally the value of β defined above is in the vicinity of one in the solar wind. The theory of collisionless shocks in $\beta \approx 1$ plasmas is still in its infancy, however. This fact further enhances the value of observational studies of the plasma physics of shocks in the solar wind.

Most studies of the plasma physics of shocks in the solar wind have dealt with the earth's bow shock. A difficulty with these bow shock studies has always been the question of the observational determination of the location of the observing satellite with respect to the shock due to the largely unknown fluctuations in shock positions. This difficulty does not exist for outward propagating interplanetary shocks in most cases. The advantages and disadvantages of bow shock studies as compared with the studies of shocks of solar origin have briefly been discussed in the more special paper by Neubauer et al. (1977) in connection with the shock of January 8, 1975.

We shall here discuss observations of the fine structure of the shock of January 6, 1975, using spectral analyzer data of the search-coil experiment and fluxgate vector data. In addition to the structure of the shock transition we
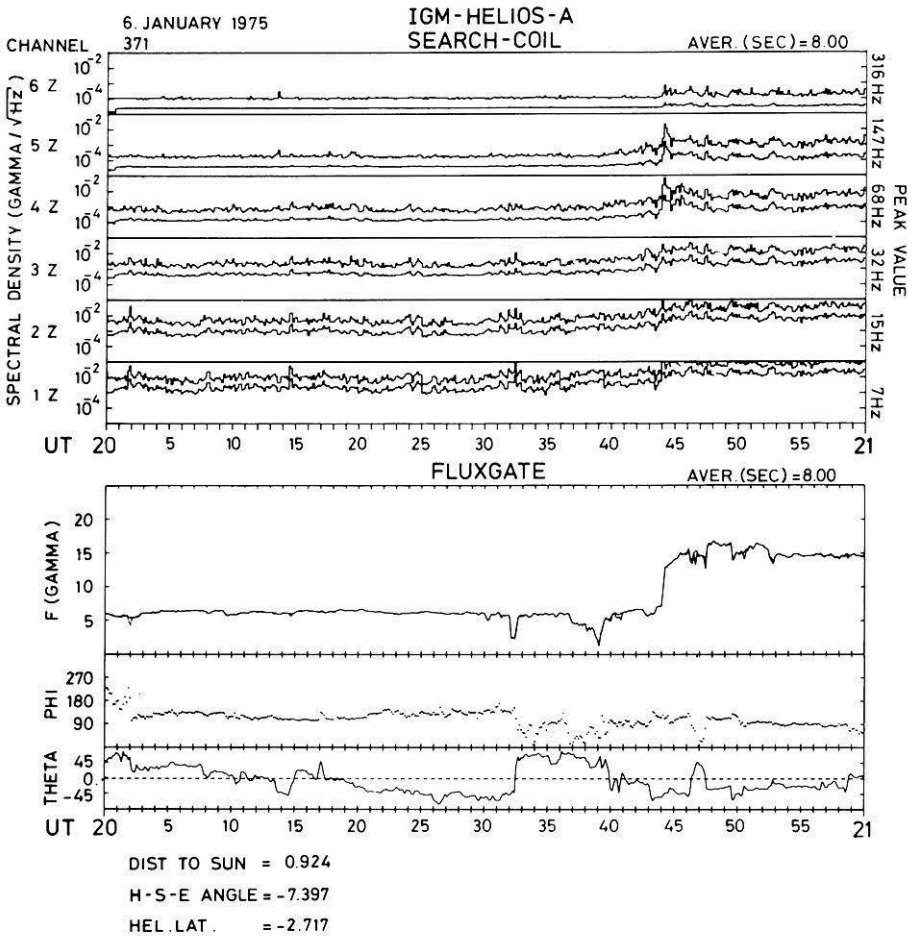
Fig. 3. Search-coil (upper panels) and flux-gate (lower panels) data for January 6, 1975, 20h–21h including the shock event

discuss the high frequency fluctuations following the shock transition and preceding it. The macroscopic properties of the overall flow system are left to a later study.

First we shall give an overview of our data in the two-hour interval containing the shock. Figures 3 and 4 show vector magnetic field data from the fluxgate experiment in the usual solar ecliptic representation with F the magnitude of the magnetic field and ϕ and θ the azimuth of the projection into the ecliptic plane and the elevation with respect to the ecliptic plane, respectively. Note also that two types of magnitude have been plotted, the magnitude of the average vector and the average of the individual magnitudes as a measure of activity within the averaging interval. The degree of agreement between both types of magnitudes is a useful measure for the amount of time variations during the averaging interval of 8 s. Figures 3 and 4 display appreciable time variations
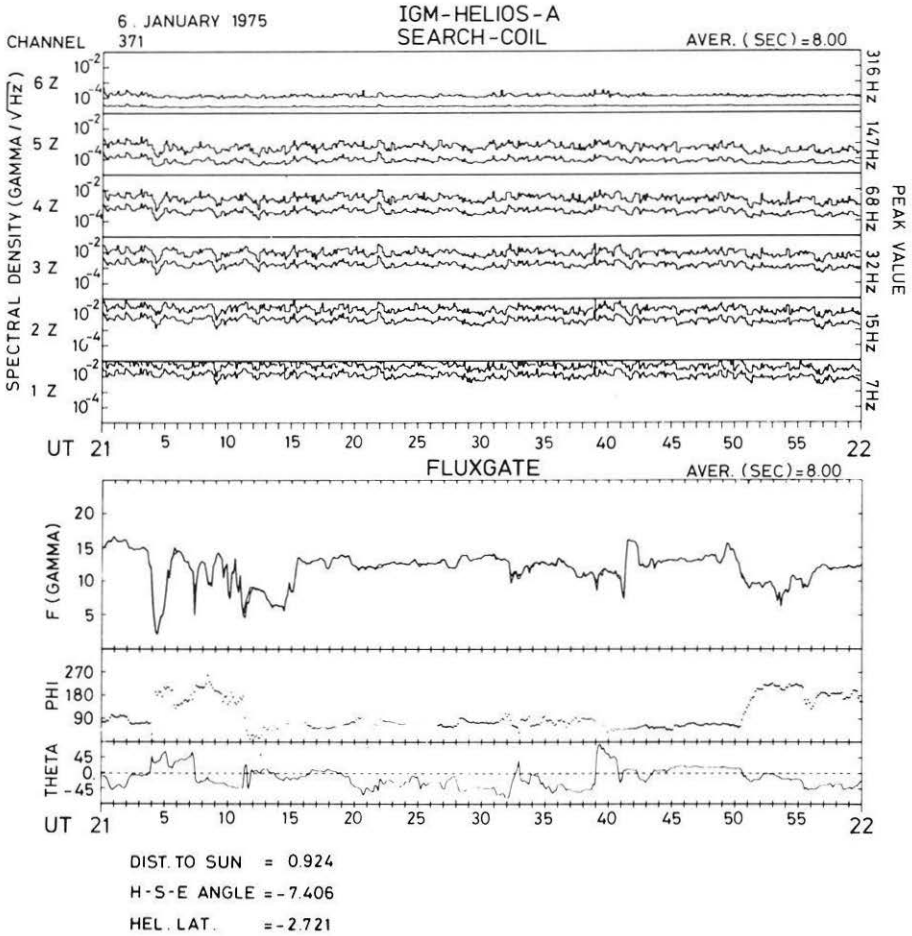
Fig. 4. Search-coil and flux-gate data for January 6, 1975, 21 h–22 h, i.e. the time interval following the shock

in the averaging interval only on a few occasions. The upper eight panels of the figures show spectral densities and peak values from the search-coil experiment for successive intervals of eight seconds which is also the averaging interval for the flux-gate data. The peak values are scaled such that for a monochromatic signal they would be above the spectral density by a factor of $\sqrt{2}$.

The shock occurs at 20 h 44 m 6 s. It is moving through a system of "magnetic holes". This name has been coined by Turner et al. (1976) for structures in the interplanetary magnetic field characterized by a strong minimum in magnetic field magnitude generally covering time intervals of several seconds. The first big one occurs at 20 h 32 m the second one at 20 h 39 m before the shock. Other magnetic holes have already been run over by the shock the most dramatic one occurring around 21 h 4 m. The magnetic holes are connected with strong variations in direction.

Let us now consider the shock transition itself. This is shown in some more detail in Figure 5. Here 4 vectors/s are plotted together with one spectrum each $T_A = 1.125$ s for the spectrum analyzer. With 20 vectors before and behind the shock we obtain

$$\bar{\mathbf{B}}_1 = (-2.59, \ 3.77, \ -5.64)\,\gamma \quad \text{and} \quad \bar{\mathbf{B}}_2 = (-4.18, \ 7.11, \ -10.00)\,\gamma$$

for the magnetic field vectors before and behind the shock, respectively. Here the coordinate system used is defined by the X-direction pointing towards the sun and the Z-direction towards the north ecliptic pole. This also defines the Y-direction. Due to an as yet unknown zero-offset the Z-component is uncertain by $\pm 2\gamma$. The difference vector $\Delta\bar{\mathbf{B}} = \bar{\mathbf{B}}_2 - \bar{\mathbf{B}}_1 = (-1.58, \ 3.34, \ -4.36)\,\gamma$ must lie in the shock plane i.e. $\Delta\bar{\mathbf{B}}\cdot\mathbf{n} = 0$, where $\mathbf{n}$ is the shock normal. The angle between $\mathbf{B}_1$ and $\mathbf{B}_2$ is always less than $7°$ if we vary the unknown offset of the Z-component. Making use of the conservation of the normal magnetic field component in a shock it is easy to show that the shock must be close to a perpendicular one. Because of the small angle between $\bar{\mathbf{B}}_1$ and $\bar{\mathbf{B}}_2$ the coplanarity theorem cannot be used to determine the normal direction.

Using plasma data (H. Grünwaldt and R. Schwenn, personal communication) and assuming a perpendicular shock a normal direction $\mathbf{n} = (-0.785, \ 0.363, \ 0.502)$ is found corresponding to the solar ecliptic angles $\phi_n = 155 \pm 15°$ and $\theta_n = 30 \pm 15°$. The shock velocity in the direction of $\mathbf{n}$ turns out to be 625 km/s.

The shock transition as observed by the flux-gate occurs between two successive vectors i.e. in less than 0.25 s. The jump is $\Delta\mathbf{B} = (-1.5, \ 2.3, \ -4.0)\,\gamma$ which is not much different from the jump in averaged vectors $\Delta\bar{\mathbf{B}}$. The jump in the magnetic vector field is followed by enhanced magnitude and particularly directional variations. Approximately 4 s after the shock transition a double spike in direction extending over 2 s occurs. During 20 more s magnetic fluctuations occur which have relatively high amplitudes and are relatively well ordered. This region is limited by a directional discontinuity with a dip in magnitude. In order to investigate the nature of the magnetic wave fields following the shock we make use of a minimum variance analysis of the Sonnerup type (Sonnerup and Cahill, 1967). Briefly, the method consists of the subtraction of the average magnetic field vector from the individual vectors during a given time interval and the subsequent determination of the eigenvectors and eigenvalues of the covariance matrix of these perturbation vectors. It has extensively been used to analyze discontinuities (e.g. Smith, 1973) and waves (e.g. Russell et al., 1971). The variance analysis applied to the time interval from 20 h 44 m 6 s–20 h 44 m 30 s yields a minimum eigenvalue of $6 \times 10^{-2}\,\gamma^2$ with an eigenvector close to the average $\mathbf{B}$-direction and a Pythagorean sum of $2.19\,\gamma^2$ for the components perpendicular to it. In other words, the variations in magnitude are only 16% of the variations perpendicular to the average vector. At least for these variations with relatively low frequency the wave modes are therefore essentially directional.

The accompanying behavior of the spectrum analyzer data is very interesting as Figure 5 shows. Ahead of the schock the magnetic fluctuations are well above
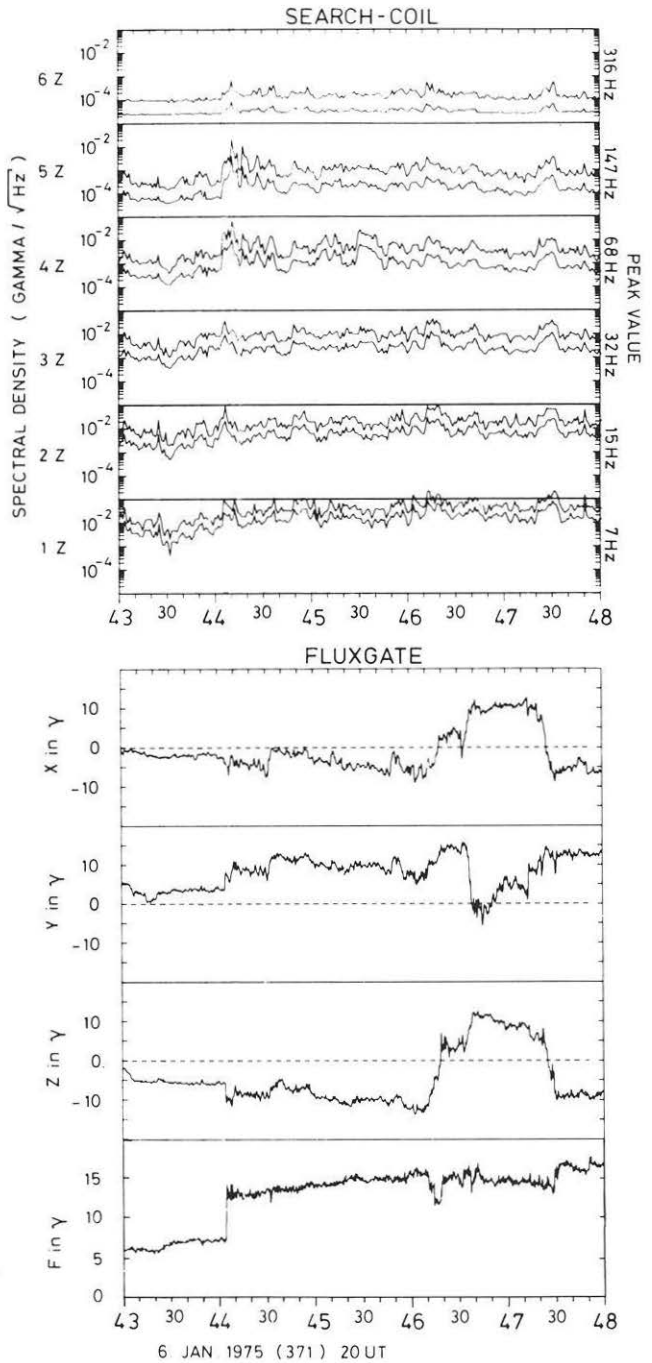
SEARCH-COIL

FLUXGATE

Fig. 5. High-time-resolution search-coil and flux-gate data around the shock of January 6, 1975

6. JAN 1975 (371) 20 UT

the background noise level except for channel 6Z around 316 Hz. At the shock transition spectral densities jump to reach a relative maximum simultaneously in all channels. The jumps are most conspicuous in the channels centered around 68 Hz and 147 Hz. In the channel around 316 Hz the noise level is just exceeded.

In order to estimate the shock thickness let us try to model it by a linear ramp of height ΔB_z and length Δt connecting 2 constant states of the magnetic field in the Z-direction. The squared time derivative of the simple ramp averaged over the basic measuring time interval T_A is given by

$$\frac{1}{T_A} \int_0^{T_A} \dot{B}_z^2 \, dt = \frac{(\Delta B_z)^2}{T_A \, \Delta t}. \tag{4}$$

The measured contribution from 4.7 Hz–220 Hz for the Z-component according to Equation 3 is

$$\overline{\dot{B}_z^2} \, (1,5) = 410 (\gamma/\text{s})^2.$$

Together with the $\Delta B_z = -4\gamma$ jump from the flux-gate within 0.25 s and Equation 4 this indicates a transit time Δt of > 30 ms for this shock. However, the ratio of peak value over spectral density can be taken as a crude indication of the nature of the signal. It is found not to be different from the ratios usually encountered for 1.125 s intervals. It seems therefore reasonable to conclude that the shock consisted of a ramp of "thickness" much greater than 30 ms but below 250 ms which is dominated by turbulent magnetic wave fields. Using the shock velocity of 625 km/s the thickness must be between 19 km and 160 km. In units of the proton gyro radius at the Alfvén speed ahead of the shock the thickness should be between 0.2 and 1.7, respectively.

Four seconds after the first jump in wave activity the maxima occur in the channels centered around 7 Hz, 68 Hz, 147 Hz and 316 Hz apparently in connection with the double spike mentioned above. Relative maxima occur in all channels except channels 7 and 8 which exhibit no activity at all. After these maxima the wave activity decreases within a few minutes to a level which remains above the preshock values for several hours. Note that for a magnetic field of $F_2 = |\overline{\mathbf{B}}_2| = 13\gamma$ the electron gyro frequency $f_{ce} = 360$ Hz. Even without the use of plasma data it is clear that for propagation perpendicular to the magnetic field these frequencies can only be reached by strongly Doppler shifted waves near the lower hybrid frequency. If waves propagating parallel to $\mathbf{B}_2$ are involved their Doppler shifts are generally small since $\overline{\mathbf{B}}_2$ is almost perpendicular to the solar wind flow direction. Such waves would then extend up to an appreciable fraction of the electron gyro frequency f_{ce}. A third possibility is the occurrence of very thin convected structures like the electron sheaths treated by Lemaire and Burlaga (1976). The wave peak region near the double spike contributes the 1.125 s averages $\overline{\dot{B}_z^2} = 2800 \, (\gamma/\text{s})^2$ in the frequency range from 47–470 Hz. For an unresolved jump in B_z by $\Delta B_z = 2\gamma$ this would correspond to $\Delta t \approx 1.3$ ms. Again the ratio peak value over spectral density suggests high levels

of broad band fluctuations as the cause of the peaks with a broad spectral maximum around 68 Hz.

It is interesting to speculate that the structure just described is a part of the shock fine structure. However, because of the somewhat disturbed conditions before the shock it can also be due to some interplanetary structure like a directional discontinuity which is overtaken by the shock. Peaks in spectral density are clearly visible in Figure 5 ahead of the shock. Small but clear signatures can also be distinguished in the magnetic field data. Since the "magnetic holes" are convected structures (Turner et al., 1976) it is reasonable to assume that some of these small fluctuations are also convected.

It is then very interesting to investigate the change of stability characteristics during the shock transition. Since the shock is perpendicular, we can easily make the following simple estimate. If the thickness of a convected structure with a normal in the direction of the shock normal is d_1 ahead of the perpendicular shock it will be

$$d_2 = \frac{F_1}{F_2} d_1 \tag{5a}$$

behind the shock. A magnetic disturbance $\mathbf{B}'$ in the direction of $\overline{\mathbf{B}}_1 \times \mathbf{n}$ changes according to

$$\mathbf{B}'_2 = \mathbf{B}'_1 \frac{F_2}{F_1}. \tag{5b}$$

The current density j then changes according to

$$j_2 = j_1 \left(\frac{F_2}{F_1}\right)^2.$$

Considering instabilities for which the relative velocity between electrons and ions in relation to the Alfvén speed is important (e.g. Gary et al., 1976) we obtain

$$M_{j,2} = M_{j,1} \left(\frac{F_2}{F_1}\right)^{1/2}$$

where $M_j = \dfrac{|\mathbf{v}_1 - \mathbf{v}_e|}{F/\sqrt{4\pi\rho}}$ with the density ρ. We have used $\rho_2/\rho_1 = F_2/F_1$ in a

perpendicular shock. This result shows that current instabilities in convected structures may be strengthened during the shock transition. A complete discussion would require inclusion of plasma densities as well as electron and proton temperatures. In our case $(F_2/F_1)^{1/2} = 1.33$ which may be sufficient to enhance some instabilities in a noticeable way.

The fluctuation levels following the shock transition decrease to levels which are well above the preshock values and continue for several hours with only a small decrease as Figures 3 and 4 indicate. An interesting question is how much of this enhanced fluctuation level is due to the transmitted fluctuations before
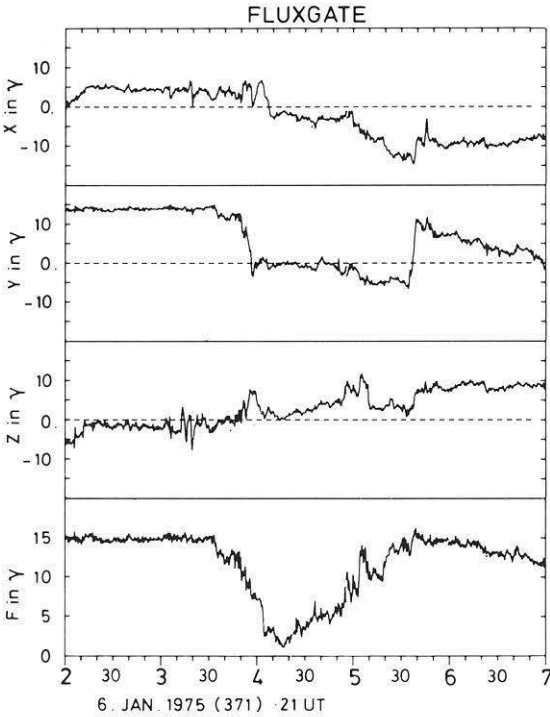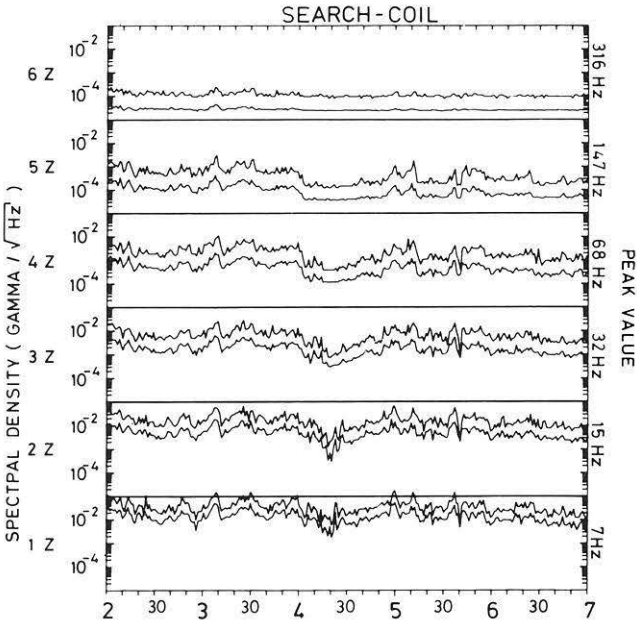
Fig. 6. "Magnetic hole" with pronounced dip in magnetic wave activity

the shock. Since the physical nature of the fluctuations has not been identified yet the question cannot be answered rigorously.

Magnetic Holes in the Vicinity of the Shock of January 6, 1975

Several magnetic holes (Turner et al., 1976) can be identified near the January 6, 1975 shock. Depending on the width and depth of the hole one might expect different kinds of observational features. In a very deep hole i.e. with a very small minimum in F, the frequency range of propagation in the plasma rest frame is very restricted because of the low electron gyro frequency. The frequency range in the satellite frame depends in addition strongly on the Doppler effect. Figure 6 shows as an interesting example the magnetic hole of 21 h 4 m in some more detail.

The narrowing of the propagation band leads to a pronounced drop in wave activity even below the background noise levels in the upper channels. At $F_{min} \approx 1\gamma \qquad f_{ce} = 28$ Hz.

If the hole is very narrow strong current densities are implied which may lead to instabilities with an electromagnetic signature. It has been suggested that in some magnetic holes merging is taking place (Turner et al., 1976). Anomalous resistivity in the merging region may be due to electromagnetic wave instabilities. This may be the reason for the very short noise spike occurring in the center of the magnetic hole starting at 20 h 32 m. The spike could also just be a consequence of the very narrow current sheet producing the directional discontinuity inside the hole without merging.

Conclusions

Initial results from the Helios-1 search-coil magnetic wave experiment have been presented. We stress the following points:

1. The low background noise levels, accurate spectral density determinations and high frequency-time resolution combined with the orbit covering 0.3–1.AU in distance allow unique studies of electromagnetic wave phenomena in the magnetoplasma of the solar wind.

2. Daily averages of the spectral densities between 0.86 AU and 0.31 AU obtained during the interval January 19, 1975 to April 5, 1975 exhibit spectra with negative slope the spectral characteristics of which do not change significantly as the sun is approached. Superposed on the increase in spectral density during the approach to the sun we find variations not clearly associated with macroscopic solar wind properties like magnetic field magnitude. In each channel spectral density variations by more than an order of magnitude (in $\gamma/\sqrt{Hz}$) have been observed.

3. As a dramatic example of the wave fields on short time scales we have investigated the shock of January 6, 20 h 44 m 6 s. Using Helios-1 flux-gate and

search-coil data the following properties have been found. The shock is close to a perpendicular one with a thickness between 19 km and 160 km but probably closer to the upper limit. In proton gyro radii at the Alfvén speed based on the plasma density before the shock the respective numbers are 0.2 and 1.7. It is followed within 4 s by a structure with a strong peak in the frequency spectrum around 68 Hz. This may either be part of the shock structure or produced by a feature in the disturbed medium into which the shock propagates.

The overall enhancement of fluctuation levels following the shock for hours may partly be due to transmitted preshock fluctuations.

4. The shock is moving into an ensemble of "magnetic holes" (Turner et al., 1976). A pronounced example of a magnetic hole with $F_{min} = 1\,\gamma$ is characterized by a significant dip in wave activity.

Another hole with a longer F_{min} but a very narrow directional discontinuity produces a pronounced wave spike.

During the discussion we have pointed to a number of interesting subjects which are presently being studied or will be studied in the future.

References

Dehmel, G., Neubauer, F.M., Lukoschus, D., Wawretzko, J., Lammers, E.: Das Induktionsspulen-Magnetometer-Experiment (E4). Raumfahrtforschung. **19**, 241–244, 1975

Galeev, A.A.: Collisionless shocks. In: Proc. Symp. on Solar Planet. Relationships, D.J. Williams, Ed., Boulder, 1976

Gary, S.P., Gerwin, R.A., Forslund, D.W.: Electromagnetic current instabilities. Phys. Fluids, **19**, 579–586, 1976

Hollweg, J.V.: Waves and instabilities in the solar wind. Rev. Geophys. Space Phys. **13**, 263–289 1975

Lemaire, J.F., Burlaga, L.F.: Diamagnetic boundary layers in the solar wind: kinetic theory. Submitted to Astrophys. Space Sci., 1976

Neubauer, F.M., Musmann, G., Dehmel, G.: Fast magnetic fluctuations in the solar wind: Helios 1. Accepted by J. Geophys. Res., 1977

Russell, C.T., Childers, D.D., Coleman, P.J.: Ogo 5 observations of upstream waves in the interplanetary medium: discrete wave pachets. J. Geophys. Res. **76**, 845–861, 1971

Schindler, K.: Laboratory experiments related to the solar wind and the magnetosphere. Rev. Geophys. **7**, 51–75, 1969

Smith, E.J.: Identification of interplanetary tangential and rotational discontinuities. J. Geophys. Res., **78**, 2054–2063, 1973

Sonnerup, B.U.Ö., Cahill, Jr., L.J.: Magnetopause structure and attitude from Explorer 12 observations, J. Geophys. Res. **72**, 171–183, 1967

Turner, J.M., Burlaga, L.F., Ness, N.F., Lemaire, J.F.: Magnetic holes in the solar wind, EOS. Trans. Am. Geophys. Union **57**, 320, 1976